JMEPEG (2009) 18:406–413
DOI: 10.1007/s11665-008-9303-8

1059-9495/$19.00

Stress Corrosion Cracking Behavior of Peened Friction Stir Welded 2195 Aluminum Alloy Joints

Omar Hatamleh, Preet M. Singh, and Hamid Garmestani

(Submitted January 29, 2008; in revised form August 4, 2008)

The surface treatment techniques of laser and shot peening were used to investigate their effect on stress corrosion cracking (SCC) in friction stir welded (FSW) 2195 aluminum alloy joints. The investigation consisted of two parts: the first part explored the peening effects on slow strain rate testing (SSRT) in a 3.5% NaCl solution, while the second part investigated the effects of peening on corrosion while submerged in a 3.5% NaCl solution with no external loads applied. For the SSRT, the laser-peened samples demonstrated superior properties to the other samples, but no signs of corrosion pitting or SCC were evident on any of the samples. For the second part of the study, the FSW plates were inspected periodically for signs of corrosion. After 60 days there were signs of corrosion pitting, but no stress corrosion cracking was noticed in any of the peened and unpeened samples.

Keywords friction stir welding, laser peening, shot peening, stress corrosion cracking, 2195

1. Introduction

Friction stir welding (FSW) was developed (Ref 1) as a promising solid-state process with encouraging results. This welding technique has potential significant application in different industrial applications (Ref 2), and has resulted in welded joints being used in critical load-bearing structures and structurally demanding applications (Ref 3). FSW transforms the metal into a plastic state at a temperature below the melting temperature of the material (Ref 4), and then mechanically stirs the material together under pressure to form a welded joint. Advantages of the FSW process for welding aluminum include elimination of consumables and the solidification zone in the weld region. This will mitigate cracking problems associated with segregation during solidification of the weld metal (Ref 5).

Since FSW takes place at a low temperature level compared to fusion welding, residual stresses in this case are generally lower than that in fusion welds. Nevertheless, the heating cycle in the material during welding, and the very rigid clamping arrangement used during FSW, can have an impact on weld residual stresses (Ref 6-8). The residual stresses developed during the welding process can have a significant effect on the service performance of the welded material (Ref 9), and can result in stress corrosion cracking (SCC) in the presence of specific environments.

Omar Hatamleh, Structures Branch, NASA – Johnson Space Center, Houston, TX 77058; and **Preet M. Singh** and **Hamid Garmestani**, School of Materials Science and Engineering, Georgia Institute of Technology, Atlanta, GA. Contact e-mail: omar.hatamleh-1@nasa.gov.

In moist environments, corrosion tends to occur in Al-Li alloys and deteriorates their mechanical properties (Ref 10). Therefore, investigating the SCC behavior under the tensile residual stresses generated through welding is necessary. For the unstressed 2195 alloy, general corrosion, intergranular corrosion, and pitting corrosion occur. As stress is applied, the intergranular corrosion is greatly aggravated, and severe general corrosion is developed from multitudinous pits (Ref 10). Consequently, introducing compressive residual stresses through peening techniques can be significantly beneficial. Shot peening is an established method by which the surface of a part is deformed plastically by multiple overlapping impacts using glass or metal spheres. The depth of the compressive residual stress is generally only around 250 μm (Ref 11). For that reason, other peening techniques that can produce deeper compressive residual stresses are needed.

Laser shock peening is a surface treatment technique capable of introducing deep compressive residual stresses to moderate the residual tensile welding stresses. The laser peening process generates a compressive residual stress at the surface that can be significantly deeper than for conventional shot peening (Ref 12, 13). This improves crack growth resistance for cracks initiating at the surface/subsurface of the peened components. The actual depths of the laser peening-induced stresses will vary depending on the material properties of the peened parts, and the processing conditions chosen (Ref 14).

In this study, shot peening and a variety of laser peening layers were used to introduce compressive residual stresses into FSW AA 2195. The surface residual stresses were characterized through x-ray diffraction, and the influence of the different peening techniques on stress corrosion cracking in FSW specimens was investigated. The first part of the study investigates the peening effects on slow strain rate testing (SSRT) in a 3.5% NaCl solution, while the second part of the study investigates the effects of peening on corrosion while submerged in a 3.5% NaCl solution with no external loads applied.

2. Experimental Setup

Aluminum alloy (AA) 2195 with 1.25 cm thickness was used for this investigation. The welding direction was aligned with the rolling direction, and the dimensions of the FSW panels after welding were 91 cm by 30 cm by 1.25 cm as illustrated in Fig. 1. The mechanical properties for the base material are as shown in Table 1.

The specimens used in this study were either shot-peened or laser-peened using different layers. The number of layers denotes the number of times the peening was repeated over a specific area of the sample. For instance, three layers correspond to the same area being treated three times. Unpeened FSW samples were also tested and used as a baseline. The shot peening process was performed using 0.59 mm glass beads with an Almen intensity of 0.008 to 0.012 A. The laser peening was applied using a square laser spot with a laser power density of 5 GW/cm^2 and 18 ns in duration at a frequency of 2.7 Hz and a wavelength of 1 micrometer. For the slow strain rate tensile samples, the gage section on all four sides of the specimens was shocked using the same conditions. For the SCC samples, an area of 10 by 5 cm on the center of the sample was peened on both sides.

The surface residual stresses were measured using the x-ray diffraction (XRD) technique. In XRD, the strain in the crystal lattice is measured assuming that the crystal lattice is linearly distorted. The atomic spacing (d) between crystallographic planes that are equal will vary consistently with their psi (ψ) angle, where the ψ angle is defined as the "angle between the surface normal and the normal to the crystallographic planes from which the x-ray peak is diffracted" (Ref 15). Therefore, to determine the magnitude of residual stresses, the lattice strains are assessed in various ψ directions and a plot of $\sin^2 \psi$ versus $\varepsilon_{\phi\psi}$ is derived (where ϕ is the angle between a reference direction and the direction of stress measurement in the plane). $\varepsilon_{\phi\psi}$ is the strain in the ϕ and ψ directions defined by (Ref 16):

$$\varepsilon_{\phi\psi} = \frac{1+\nu}{E}\left(\sigma_\phi \sin^2 \psi\right) - \frac{\nu}{E}(\sigma_1 + \sigma_2) \qquad \text{(Eq 1)}$$

where ν = Poisson's ratio; σ_ϕ = surface stress at ϕ angle with a principal stress direction; E = modulus of elasticity; σ_1, σ_2 = principal stresses.

Then, from the $\sin^2 \psi$ versus $\varepsilon_{\phi\psi}$ plot, residual stresses are established through the following relation:

$$\sigma_\phi = \frac{mE}{1+\nu} \qquad \text{(Eq 2)}$$

where m = slope of the $\sin^2 \psi$ versus $\varepsilon_{\phi\psi}$ plot.

Residual stresses were acquired using a Philips X'Pert PW3040 MRD X-ray diffractometer, operating at 40 kV and 45 mA, and employing Ni-filtered Cu K-α radiation. The measurements were taken using 2θ scans from 77 to 79°, with 0.01° per step and 1 s per step, (311) peak positions at 10 different tilt angles.

For the slow strain rate testing (SSRT), transverse tensile specimens 20 cm long with a gage length of 8.5 cm and a gage width of 1.25 cm were used. The tensile samples were oriented such that the weld was in the center of the specimen and the load was applied perpendicular to the weld direction. The gage portion of the tensile samples was submerged in a 3.5% NaCl solution at room temperature and was placed in a servo-hydraulic universal testing machine. SSRT tests were carried out at an initial strain rate of 2×10^{-6} mm/s. Tests were also carried out to examine the effect of residual stresses on the possibility of initiation and propagation of stress corrosion cracks. For these tests, the welded samples with dimensions of 41 by 10 cm wide were used. The samples were placed in a 3.5% NaCl solution, and they were inspected periodically for evidence of stress corrosion cracking or corrosion pitting. One sample was used for testing under each peened condition.

In general, aluminum alloys can fail by cracking along grain boundaries when simultaneously exposed to specific environments and stresses of sufficient magnitude. Stresses sufficient for crack initiation and crack growth can be far below the stresses required for gross yielding. The stress-corrosion

Table 1 Tensile properties for the as-received AA 2195-T8

Material	0.2% Yield stress, MPa	Ultimate strength, MPa
2195-T8	503	537

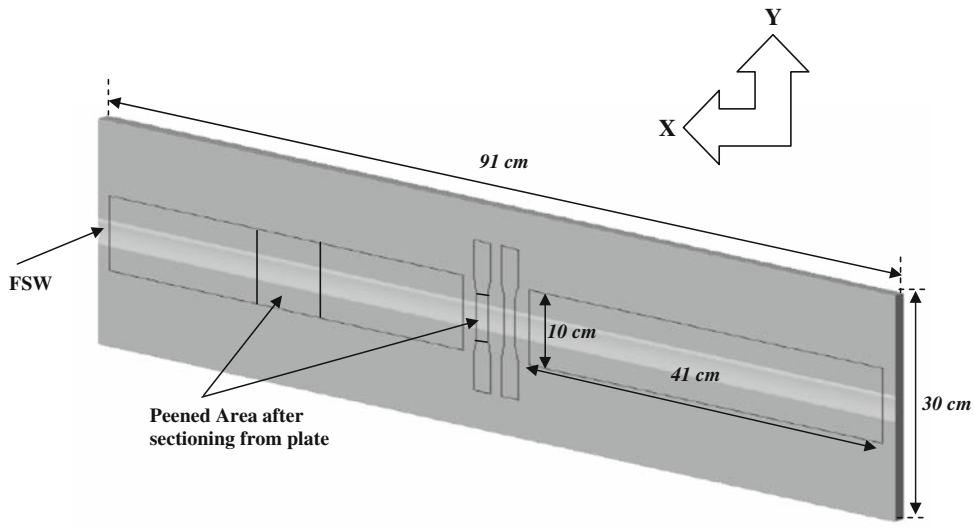

Fig. 1 Specimens used for the SCC testing

cracking in aluminum alloys is characteristically intergranular. The benefit of slow strain rate testing is that it produces results in a reasonably short time depending on strain rate. It also reduces incubation time to the onset of cracking in susceptible materials. The plastic strain causes an accelerated disruption of surface films thereby overcoming the initial period of incubation that can result in unacceptably long test durations.

3. Results and Discussion

3.1 Weld Microstructure

A micrograph illustrating different regions of the weld is shown in Fig. 2. The weld nugget appeared to be wider on the crown region of the weld since the upper surface is in contact with the tool shoulder. The grain structure at the thermo mechanical affected zone (TMAZ) was elongated and distorted due to the mechanical action from the welding tool. The grain structure in the heat affected zone (HAZ) resembles the parent material grain structure, although the precipitates in this region are generally larger than in the base material.

3.2 Mechanical Properties and Hardness

The tensile properties at different regions across the weld are illustrated in Fig. 3. From the graph, it is clear that the weld nugget exhibited the lowest yield strength when compared to other locations across the weld. This may be attributed to the fact that the original structure in this region is over-aged and there is not enough solute left in the material. Therefore, this region of the weld will be relatively ineffective in inhibiting dislocation motion, and the resultant strain localization in the softened area of the weld will result in lower mechanical properties. In addition to these microstructural changes, the residual stresses in the weld region may have had an effect on the tensile properties in the samples.

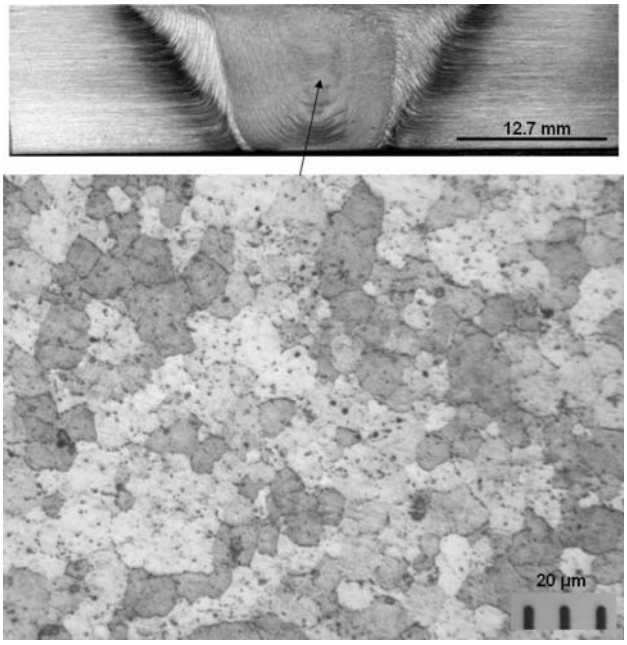

Fig. 2 Metallographic cross section of 2195 friction stir weld

Due to the heat generated during the welding process, the dislocation density in the nugget is generally lower than in the parent material. Since the strengthening precipitates appear to have solutionized during the welding process (Ref 17, 18), this indicates that the temperature during joining was above the solution temperature of the hardening precipitates. It is also clear that the yield strength at the weld interface was lower than the corresponding properties in the HAZ. The properties at the TMAZ on both sides of the weld (advancing and retreating) were similar. Since the yield strength of the transversely loaded FSW specimens is less than the yield strength of the base metal, the base metal experienced predominantly elastic strain throughout the test (Ref 2).

To examine the strains across the weld region for the unpeened FSW specimens, the strain field in the x direction before failure was recorded and is shown in Fig. 4. The strain field was acquired from the tensile testing through the ARAMIS system. It is clear that the highest strain concentration took place in the weld nugget, which is where the failure occurred. The maximum strain before failure was around 12.6%.

To assess the hardness across the weld region, hardness measurements shown in Fig. 5 were taken using a Struers Duramin A-300 Knoop microhardness tester, using a dwell (load time) set to 3 s. Softening was noted throughout the weld zone, probably due to coarsening and dissolution of strengthening precipitates induced by the thermal cycle of the FSW. For example, Li and Oertelt (Ref 17, 18) reported that in AA 2195 the strengthening precipitates like T1 were no longer present in the weld nugget. The T1 is considered to be the primary strengthening precipitate in the 2195 alloy (Ref 19). Away from the weld nugget, hardness levels increased with increasing distance as precipitation hardening became more effective. All peened areas on the samples experienced some levels of work hardening depending on the peening conditions. A detailed investigation on the effects of peening on hardness in FSW is discussed in (Ref 20).

3.3 Residual Stress

The surface residual stresses at different distances in the weld nugget region for the tensile specimens are outlined in Fig. 6. The stresses are shown for the various peening conditions used in this study. In general, all the peening techniques resulted in high surface compressive stresses, with

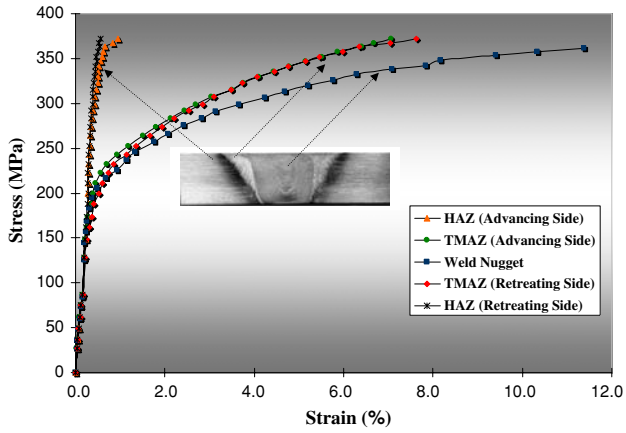

Fig. 3 Tensile properties at different regions of the weld for FSW 2195 AA

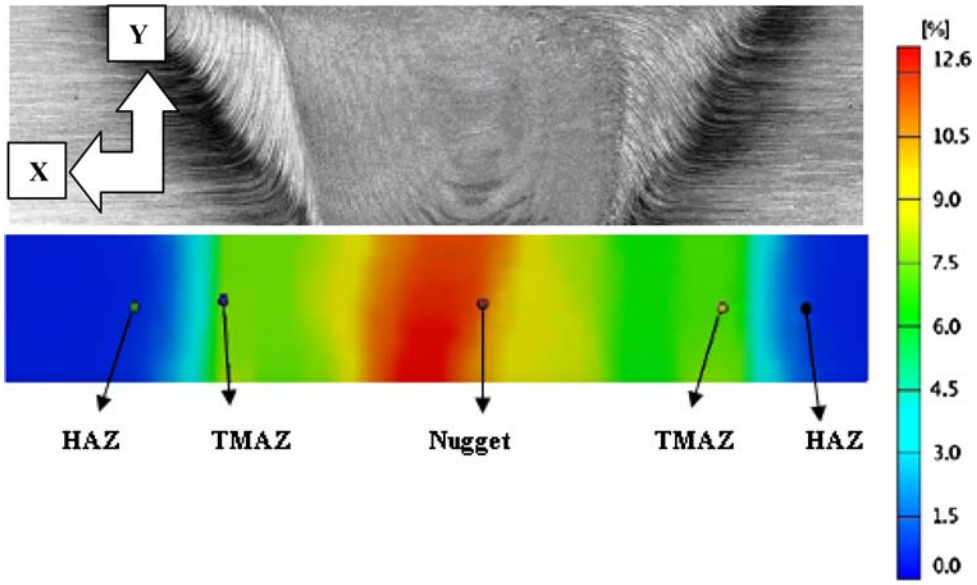

Fig. 4 Strain fields in the *x* direction for the specimen before failure

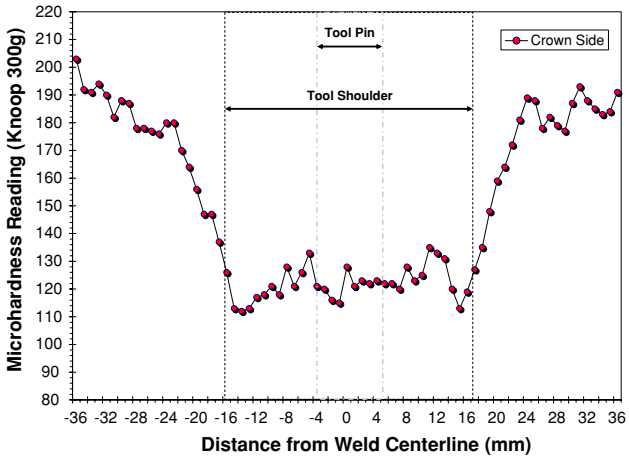

Fig. 5 The microhardness profile across the weld region for FSW 2195

shot peening yielding the highest stresses for all the measured regions. This is probably due to the high amount of cold work generally produced by shot peening. Even though the highest surface stresses were attained by shot peening, it is expected that laser peening produced compressive stresses significantly deeper. It was also noticed that the residual stresses in the longitudinal and transverse direction did not vary by an appreciable amount.

3.4 Stress Corrosion Cracking (SCC) Susceptibility

The tensile samples were tested by SSRT method in 3.5% NaCl solution at room temperature with an initial strain rate of 2×10^{-6}/s. Mechanical behavior of the tested samples is shown in Fig. 7. Fractured samples after tests were used to determine the percent reduction in area and the percent elongation, which are listed in Table 2. Tested samples did not show any signs of surface cracks throughout the gage length. All tested tensile samples of AA 2195 fractured in the nugget region. Hardness results shown in Fig. 5 indicate that the hardness and strength of the weld nugget region and TMAZ was lower than the base metal regions. According to Hu and Meletis (Ref 21) the temperatures during FSW are in the range of 400 to 480 °C and the T1 (Al_2CuLi) phase present in AA 2195 is redissolved, putting Cu back in solid solution, thereby decreasing the strength of the nugget and adjacent areas. The final fracture in the absence of any environmental effect is expected to be in the region of lower strength. Results in Fig. 7 and Table 2 show an improvement in ultimate stress from using laser peening; however, percent elongation and percent reduction in area for the sample with 6-laser peening layer was lower than that for the other samples.

Hu and Meletis (Ref 21) investigated stress corrosion cracking behavior of AA 2195 in 3.5% NaCl solution using the SSRT method as well as constant load tests (four point bend tests). Their samples were not surface treated, and they reported that environment-induced cracking was observed only by the SSRT method. Flat brittle fracture morphology with no signs of corrosion was observed several hundred micrometers around pits formed on the samples. They attributed this fracture morphology to the hydrogen embrittlement where hydrogen is produced by the corrosion process. The fracture surface analysis showed that for all specimens, the fracture initiated at the bottom line of the weld, which showed evidence of a very thin layer of incomplete welding. However, no such cracks were seen on the SSRT samples tested in the present study. Hu et al. reported that the constant load tests up to stress levels ~90% of the yield strength for a 90-day exposure indicated that the stir welded samples were not susceptible to stress-corrosion cracking. No pitting attack on test samples was reported after the 90-day exposure.

Examination of SSRT samples from the present study under an optical microscope did not show any signs of pitting or intergranular attack on the surface of SSRT samples in 3.5% NaCl solution. Average test duration for the SSRT was less than 24 h, which was relatively short exposure time for the alloys to show significant pits. Initial strain rate affects stress corrosion cracking susceptibility in SSRT method. To investigate this

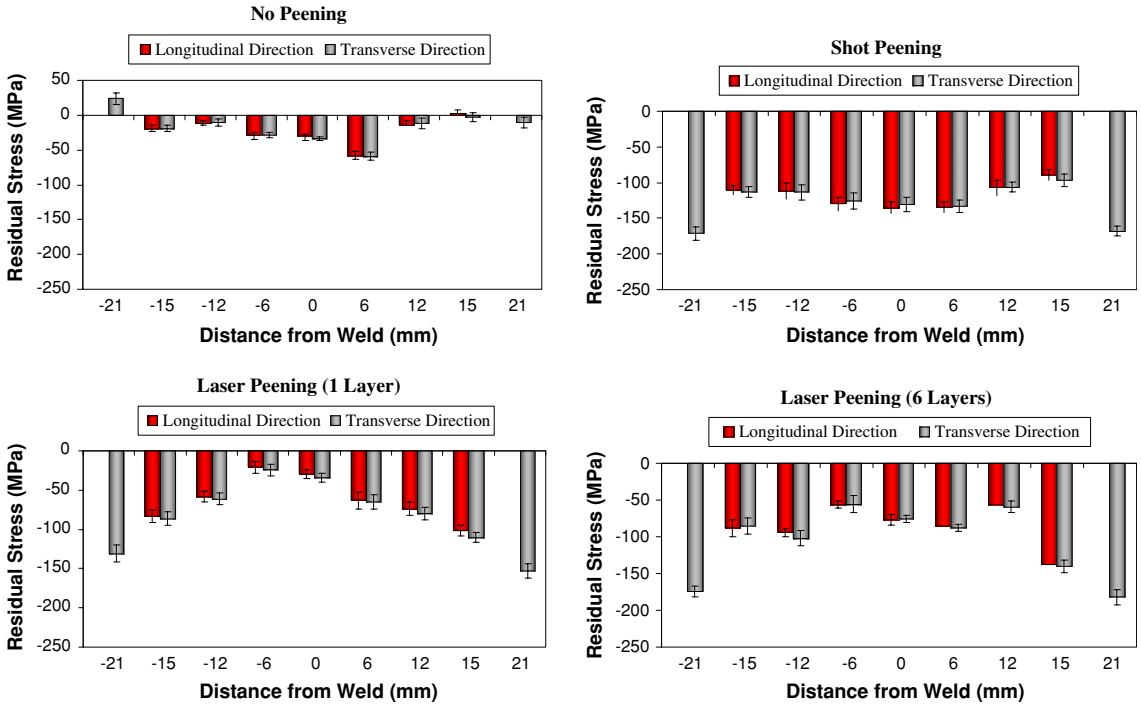

Fig. 6 Residual stresses for different peening conditions across the weld

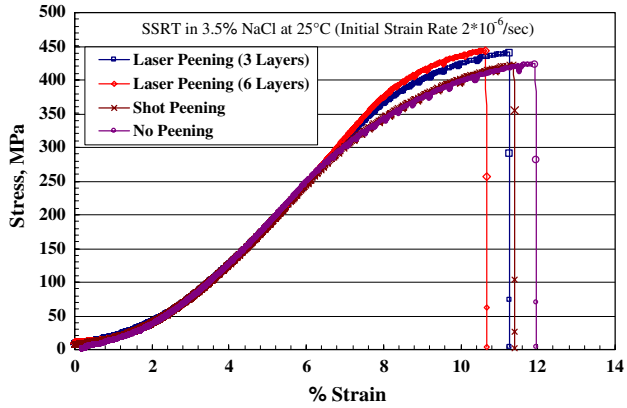

Fig. 7 Stress-Strain behavior for stir welded AA 2195 samples with different surface treatments tested by SSRT method in 3.5% NaCl solution at initial strain rate of 2×10^{-6}/s

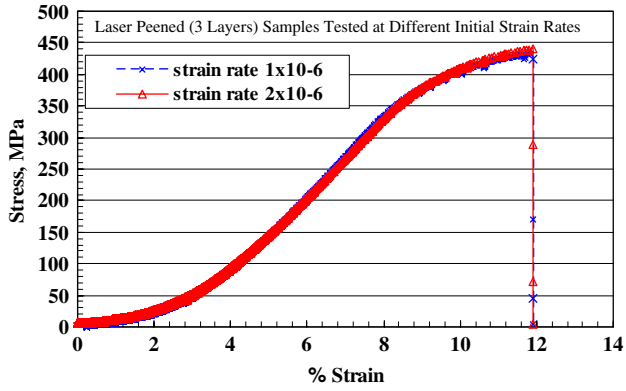

Fig. 8 Stress-Strain behavior AA 2195 samples tested by SSRT method in 3.5% NaCl solution at different initial strain rates

Table 2 Summary of slow strain rate test results for 2195 tensile samples tested in 3.5% NaCl solution at room temperature

Materials	Initial strain rate, s^{-1}	Ultimate tensile strength, MPa	% Area reduction	% Elongation	Stress corrosion cracking susceptibility
Laser peening (3 layers)	1×10^{-6}	432.2	18.37	4.10	No SCC
Laser peening (3 layers)	2×10^{-6}	440.0	12.99	4.01	No SCC
Laser peening (6 layers)	2×10^{-6}	444.2	10.64	3.01	No SCC
Shot peening	2×10^{-6}	423.0	13.68	4.27	No SCC
No peening	2×10^{-6}	423.5	15.30	5.27	No SCC

effect and allow longer exposure time, a AA 2195 sample with 3 laser peening layers was also tested with an initial strain rate of 1×10^{-6}/s. However, the results indicated that there was no difference in the mechanical behavior of the two test samples, as shown in Fig. 8, and neither samples showed any sign of stress corrosion cracking.

Table 3 General corrosion of welded AA 2195 bars exposed to 3.5% NaCl solution at room temperature for 2 months

Sample	Surface area, in^2	Initial weight, g	Final weight, g	Weight change, g	Corrosion rate, mpy
Unpeened	147.95	1431.7	1431.4	0.3	0.27
Laser peened (3 layers)	148.45	1423.6	1423.3	0.3	0.27
Shot peened	147.97	1435	1434.7	0.3	0.27

Table 4 Pitting corrosion and SCC susceptibility of welded AA 2195 bars exposed to 3.5% NaCl solution at room temperature

Sample ID	Top side (welded) after 1 month	Bottom side after 1 month	Surface cracking after 1 month	Surface cracking after 2 months
Unpeened	Pitting	Pitting	No cracks	No crack
Laser peened (3 layers)	Few pits	Few pits	No crack	No crack
Shot peened	No pitting	Few pits	No crack	No crack

Unstressed 1.25 cm thick AA 2195 stir welded bars were exposed to 3.5% NaCl solution at room temperature for a 60-day period to evaluate their tendency to general corrosion, pitting corrosion, and stress corrosion cracking. Samples were examined every week for localized attack and surface stress corrosion cracks on and near the weld region. After 1 week of exposure, AA 2195 samples started showing some signs of surface pit initiation where the pit density and size increased with time. Test bars were weighed before and after the test, and the weight change was used to calculate the general corrosion rate. The calculated general corrosion rates and the corrosion susceptibility for the samples are listed in Table 3 and 4. General corrosion rates were very small for all samples, in spite of the pitting attack.

Active pitting was observed on the unpeened and the laser-peened welded samples, but very few pits were observed in the shot-peened sample. A few pits on the shot-peened sample were only on the welded (Top) side of the sample, whereas no pits were observed on the back side. Optical micrographs comparing the general and localized corrosion effects on the weld region of the FSW samples are shown in Fig. 9 for as-welded samples and after different peening conditions. The micrographs in Fig. 9 were taken after 60 days of exposure to 3.5% NaCl solution at room temperature. These samples were also observed after a 30-day exposure. The samples were air-dried and observed within a few minutes of taking out of the test solution. On the samples on which pits were detected, bubbles were seen forming at the pit mouth when observed under optical microscope. These bubbles may be due to hydrogen formed by cathodic reaction near active pit sites.

Figure 9 also shows that corrosion pitting attack was found mostly at the weld ridges that are created during the FSW process. Image analysis was used to quantify average number of pits on differently treated weld regions. For untreated weld sample, there were about 8 pits per square inch, whereas for the laser-peened sample the pit density was about 2 pits per square inch. Even after the laser-peening treatment, most of the pits were observed at the prior ridges formed by stir welding. Weld ridges were not visible on the shot-peened surface. Very few pits were observed on the shot-peened sample, but when detected, the pits on the shot-peened surface were very small compared to other surfaces.

Generally, aluminum alloy 2195, which is an age-strengthened alloy, has better pitting resistance than other aluminum alloys due to lower Cu content, but it is not immune from pitting corrosion. A lower Cu content can result in lower volume fraction of T1 (Al_2CuLi) precipitates that may also have a smaller potential difference with the Al matrix compared to the θ′ (Al_2Cu) precipitates present in alloys with higher Cu content.

The main types of precipitates in AA2195 are T1 (Al_2CuLi) precipitates growing primarily at 111 habit planes, and θ′ (Al_2Cu) tend to appear at dislocations and subgrains whereas phase T2 (Al_6CuLi_3) precipitates along grain boundaries. During the precipitation of θ′, T1, and T2, a Cu and Li depleted precipitate free zone is formed along grain boundaries and subgrain boundaries due to the absorption of Cu and Li atoms by T1, T2, and θ′ phases (Ref 22, 23).

Li et al. (Ref 10) studied the mechanism of T1 in the localized corrosion of 2195 Al-Li alloy in neutral NaCl solution. It is found that T1 acts as the main anodic phase during the initial stage of corrosion. This situation forms microscopic galvanic cells, each consisting of a large cathode and a small anode. The small anode/cathode area ratio results in a high anodic current density, thereby initiating pits in a chloride environment. In the present study, pits were generally surrounded by a circular area with different shading, which may be the local cathodic area associated with each active pit. Li et al. (Ref 10) suggested that at the later stage, the potential of T1 moves to a positive direction and becomes cathodic to the adjacent alloy base due to the preferential dissolution of Li from T1. It is suggested that the association of corrosion with T1 is caused by the alternate anodic dissolution of T1 and its adjacent alloy base, which accelerates the corrosion of the alloy base. As discussed earlier, the T1 phase present in AA 2195 will redissolve due to the temperature range in the FSW process putting Cu back in solid solution. This may further decrease the pitting tendency of the stir welded nugget.

None of the welded sample bars showed any signs of stress corrosion cracking after 2 months of exposure to chloride solution, as shown by the data in Table 2. Middle portions of these welded bar samples were surface treated by shot peening or laser peening, which causes compressive stress at the surface, as is shown by results in Fig. 6. No cracks are expected in the area of

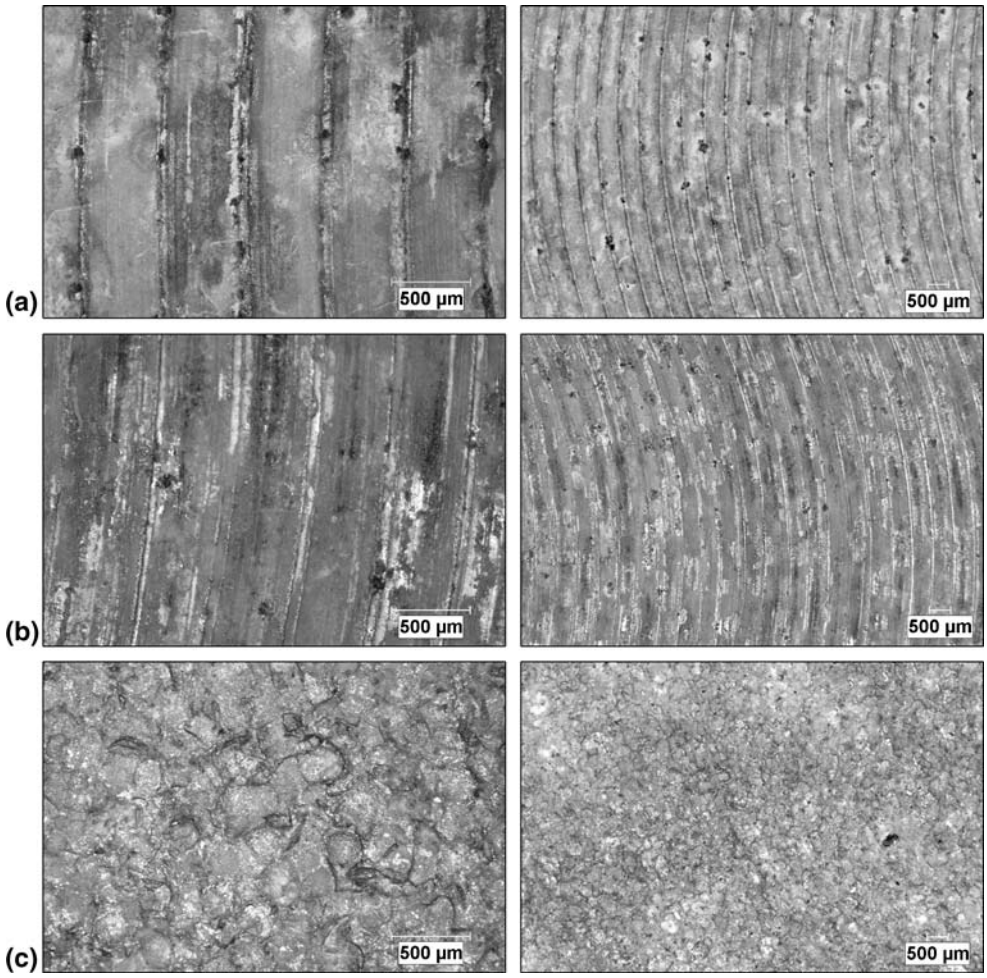

Fig. 9 Surface pits on the welded region without any peening treatment after 30 days of exposure to 3.5% NaCl solution at room temperature. (a) Welded region of the 2195 stir welded sample, without any peening, (b) Laser-peened welded region of the FSW 2195 sample, and (c) Shot-peened welded region of the FSW 2195 sample

compressive stress at the surface; however, no cracks were found even in the areas without any surface treatment. These results are similar to the ones reported by Hu and Meletis (Ref 21), where constant load test bars did not show any SCC after 90-day exposure under constant four point bend conditions.

4. Conclusion

1. Samples processed with laser peening exhibited superior tensile properties as compared to the unpeened or shot-peened samples.
2. Initial strain rate had no effect on the mechanical behavior of the samples tested under slow strain rate testing.
3. No evidence of pitting or intergranular attack was identified on the surface of SSRT samples in a 3.5% NaCl solution.
4. The unstressed FSW 2195 AA bars exposed to 3.5% NaCl solution at room temperature for a 60-day period did not have signs of stress corrosion cracking for the conditions tested in this investigation.
5. In spite of the pitting attack, results indicate that the general corrosion rates were very small for all tested samples.
6. Active pitting was observed on all friction stir welded samples except for the shot-peened sample.

References

1. W.M. Thomas, E.D. Nicholas, J.C. Needham, M.G. Murch, P. Temple-Smith, and C.J. Dawes, "Friction Stir Butt Welding," Int Patent App PCT/GB92/02203, and GB Patent App 9125978.8, 297 US patent No. 5, 460,317, October 1995
2. M. Peel, A. Steuwer, M. Preuss, and P.J. Withers, Microstructure, Mechanical Properties and Residual Stresses as a Function of Welding Speed in Aluminum AA5083 Friction Stir Welds, *Acta Mater.*, 2003, **51**, p 4791–4801
3. P. Cavaliere, Effect of Friction Stir Processing on the Fatigue Properties of a Zr-modified 2014 Aluminum Alloy, *Mater. Character.*, 2006, **57**(2), p 100–104
4. P. Staron, M. Kocak, S. Williams, and A. Wescott, Residual Stress in Friction Stir-welded A1 Sheets, *Phys. B: Condens. Matter*, 2004, **350**(1-3 Suppl. 1), p e491–e493
5. M.A. Sutton, A.P. Reynolds, D.-Q. Wang, and C.R. Hubbard, A Study of Residual Stresses and Microstructure in 2024-T3 Aluminum Friction Stir Butt Welds, *J. Eng. Mater. Technol.*, 2002, **124**, p 215–221
6. T. Ghidini and C.D. Donne, Fatigue Crack Propagation Assessment Based on Residual Stresses Obtained Through Cut-compliance Technique, *Fatigue Fract. Eng. Mater. Struct.*, 2007, **30**(3), p 214–222
7. R.S. Mishra and Z. Ma, Friction Stir Welding and Processing, *Mater. Sci. Eng. R*, 2005, **50**, p 1–78

8. C.D. Donne, E. Lima, J. Wegener, A. Pyzalla, and T. Buslaps, Investigations on Residual Stresses in Friction Stir Welds, *3'rd International Symposium on Friction Stir Welding*, Kobe, Japan, 2001
9. M.A. Sutton, B. Yang, A.P. Reynolds, and R. Taylor, "Preliminary Studies of Mixed Mode Fracture in 2024-T3 Friction Stir Welds," *Best of Aeromat Session*, ASM Materials Solutions Conference & Exhibition, St. Louis, MO, October 9-12 2000
10. F. Li, W. Chen, X. Zhao, W. Ren, and Z. Zheng, Corrosion Behavior of 2195 and 1420 Al-Li Alloys in Neutral 3.5% NaCl Solution Under Tensile Stress, *Trans. Nonferrous Met. Soc. China*, 2006, **16**, p 1171–1177
11. A. King, A. Steuwer, C. Woodward, and P.J. Withers, Effects of Fatigue and Fretting on Residual Stresses Introduced by Laser Shock Peening, *Mater. Sci. Eng. A*, 2006, **435-436**, p 12–18
12. C.S. Montross, T. Wei, L. Ye, G. Clarck, and Y.M. Mai, Laser Shock Processing, its Effects on Microstructure, Properties of Metal Alloys a Review, *Int. J. Fatigue*, 2002, **24**, p 1021–1036
13. P. Peyre, R. Fabbro, P. Merrien, and H.P. Lieurade, Laser Shock Processing of Aluminium Alloys. Application to High Cycle Fatigue Behaviour, *Mater. Sci. Eng. A*, 1996, **210**, p 102–113
14. K. Gregory, H.J. Rack, and D. Eylon, eds., *Surface Performance of Titanium*, TMS, Warrendale, PA, 1996, p 217–230
15. C.O. Ruud and D.F. Carpenter, *Operators Manual for the D-1000 - A Stress Analyzer*, Denver X-Ray Instruments, Incorporated, Englewood, 1985
16. M.E. Hilley, J.A. Larson, C.F. Jatczak, and R.E. Ricklefs, eds., "Residual Stress Measurement by X-ray Diffraction" SAE Report J784a, Society of Automotive Engineers, Inc., New York, 1971
17. Z. Li, J. Arbegast, P. Hartley, and E. Meletis, *Proceedings of the 5'th International Conference on Trends in Weldin Research*, ASM International, Materials Park, OH, 1999, p 568–573
18. G. Oertelt, S.S. Babu, S.A. David, and E.A. Kenik, Effect of Thermal Cycling on Friction Stir Welds of 2195 Aluminum Alloy, *Weld J.*, 2001, **80**(3), p 71s–79s
19. H.R. Kroninger and A.P. Reynolds, R-Curve Behaviour of Friction Stir Welds in Aluminum-Lithium Alloy 2195, *Fatigue Fract. Eng. Mater. Struct.*, 2002, **25**(3), p 283–290
20. O. Hatamleh, Surface Hardness Changes in Laser Peened Friction Stir Welded 2195 and 7075 Aluminum Alloys, *Int. J. Surface Sci. Eng.*, 2008, **2**(1-2), p 14–28
21. W. Hu and E. Meletis, Corrosion and Environment-Assisted Cracking Behaviour of Friction Stir Weded Al 2195 and Al 2219 Alloys, *Mater. Sci. Forum*, 2000, **331-337**, p 1683–1688
22. K. Kumar, S. Brown, and J. Pickens, Microstructure Evolution During Aging of an Al-Cu-Li-Ag-Mg-Zr Alloy, *Acta Mater.*, 1996, **44**(5), p 1899–1915
23. P. Niskanen, T. Sanders, and J. Kinker, Corrosion of Aluminum Alloys Containing Lithium, *Corros. Sci.*, 1982, **22**(4), p 283–304